Brightness Temperature of Lunar Surface for Calibration of Multichannel Millimeter-Wave Radiometer of Geosynchronous FY-4M

Niutao Liu, Wenzhe Fa, *Member, IEEE*, and Ya-Qiu Jin, *Life Fellow, IEEE*

***Abstract*— One of Chinese meteorological satellites, Feng Yun-4M (FY-4M), as one the of new generation of geosynchronous series satellites, is planning to upload multichannel millimeter-wave radiometers, e.g., from 50 to 430 GHz. Due to long-period stability and no atmospheric interference, brightness temperature (TB) of the lunar surface can be seen as a good candidate for thermal calibration of FY-4M radiometers. In this paper, the physical temperature profile of lunar regolith media is first derived by resolving 1-D heat transfer equation with validation of the measurements of the Diviner lunar radiometer experiment onboard the lunar reconnaissance orbiter. Then, the loss tangent is fit and validated using the TiO_2 abundances, which is derived from Clementine five-band multispectral data and Chinese Chang'e-2 37-GHz TB data. Multichannel TB of a lunar surface region along the moon equator at certain lunar time (noon and midnight) is numerically derived for all FY-4M channels. TB of lunar equator center area (0°N, 0°E) is presented with variation of the lunar local time. These results can be well applied to calibration of FY-4M, with a sustainable error in the range of 1.8 (425 GHz) to 3.8 K (89 GHz).**

***Index Terms*— Calibration, geosynchronous Feng Yun-4M (FY-4M), lunar regolith media, multichannel millimeter wave, brightness temperature (TB).**

I. Introduction

As a new generation of geosynchronous satellites for meteorological remote sensing, the first satellites of Chinese FY-2A and FY-4 programs (FY: Feng-Yun means wind cloud) had been launched in 1997 and 2016, respectively. A new one of these series is Feng Yun-4M (FY-4M) (M denotes millimeter) satellite for meteorological observations. Six millimeter-wave radiometers, i.e., 55, 89, 118, 166, 183, and 425 GHz, are planning to be uploaded. It will significantly improve the ability of monitoring and forecasting dynamic weather phenomena, e.g., typhoon, with high temporal and spatial resolutions. Quantitative accuracy of brightness temperature (TB) in observation depends on calibration techniques. Calibration is carried out before the launch in thermal/vacuum (T/V) chamber and in operations on orbit. Cold cosmos is one target for cold calibration and another target for thermal calibration can be the moon. Because there are no atmospheric interference and no quick geological variation, the moon can keep good stability of physical and chemical properties for long term. Thermal emission of lunar surface media and its TB are periodic, applicable to calibration [1].

The earliest ground-based observation of microwave TB of the moon can date back to the early 1940s [2]. However, those TBs would not be well interpreted because there were too many unknowns, e.g., the temperature profile and dielectric property of the lunar regolith media. During recent decades, advances of several satellite-born lunar remote sensing programs, especially for infrared (IR) measurements, contribute to quantitative description of thermo-physical properties of lunar regolith media at certain depth. The Diviner lunar radiometer experiment onboard the lunar reconnaissance orbiter (LRO) investigated solar reflectance and mid-IR irradiance globally [3]. Surface temperature at night can be determined by the thermo-physical properties of the regolith media, which determines the temperature profile as well. Thus, 1-D thermal conduction equation was solved to study the thermophysical properties [4], and an exponential parameter, H, was used to describe the bulk density and heat conductivity profiles [5]. Validations by surface temperature at night and temperature at deep layer from Apollo heat-flow experiment well certified that the temperature profile derived by these parameters are reasonable and applicable to calculation of TB. In 2007 and 2010, China launched Chang'e-1 (CE-1) and Chang'E-2 (CE-2) with four-channel microwave radiometers (MRM) for first observation of microwave thermal emission of lunar regolith media. Microwave of these channels can reach the layer depth about 3–5 m [6], [7].

In this paper, as the first step, based on the parameterized works [5], including the bulk density, heat conductivity, and heat capacity profiles, the temperature profiles are solved and validated with fusion of divine data and Apollo temperature measurements. Next, the dielectric properties, especially the loss tangent, are fit and validated by CE-2 37-GHz TB data. As an initial validation, simulated TB at 37 GHz (TB_{37}) are well matched with CE-2 data within the moon latitude of ±60°. Then, it is extended to the simulation of multichannel

Manuscript received June 26, 2018; revised September 3, 2018 and October 27, 2018; accepted November 5, 2018. Date of publication December 5, 2018; date of current version April 22, 2019. This work was supported in part by the National Science Foundation of China under Grant NSFC 61471127. *(Corresponding author: Ya-Qiu Jin.)*

N. Liu and Y.-Q. Jin are with the Key Laboratory of Information Science of Electromagnetic Waves, Fudan University, Shanghai 200433, China (e-mail: yqjin@fudan.edu.cn).

W. Fa is with the Institute of Remote Sensing and GIS, Peking University, Beijing 100871, China

Color versions of one or more of the figures in this paper are available online at http://ieeexplore.ieee.org.

Digital Object Identifier 10.1109/TGRS.2018.2880116

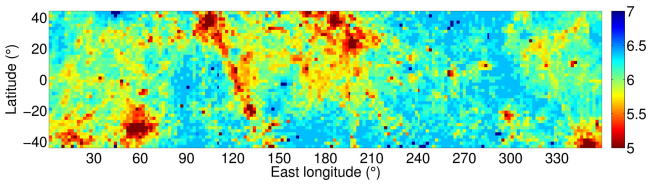

Fig. 1. Inverted H-parameters from [5]. The unit of color bar is centimeter.

millimeter-wave TB of the moon surface. Numerical analysis is carried out for thermal calibration of FY-4M program. In this paper, the Diviner data, digital elevation model (DEM), Clementine data, and Apollo heat experiment data are adopted from the planetary data system.

This paper is organized as follows. As the first step, Section II gives the calculation of physical temperature profile of regolith media with validation of Diviner data. Section III introduces the FY-4M mission and calibration using nadir observation of millimeter-wave emission of lunar surface. Section IV provides the fit loss tangent by CE-2 TB_{37} data and simulation validation. Section V presents the TB of FY-4M radiometers for calibration. Then Section VI discusses the possible errors from the uncertainty of thermo-physical and dielectric parameters, and proposes advice for future calibration. At last, Section VII gives the conclusion.

II. Physical Temperature of Lunar Surface Media With Validation of Diviner Data

A. Regolith Media With Density Profile

Lunar regolith media has been modeled as uniformly inhomogeneous with a density profile $\rho(z)$, which is described by an exponential parameter H [5]. It governs the regolith bulk density and heat conductivity and as a result, contributes to final thermal emission from the regolith media. It was found that the parameter H along the equator is in the range of 0.055–0.065 m, with the mean value of 0.06 m. Based on the study of Diviner data and Apollo lunar soil samples, the density profile has been proposed as [5]

$$\rho(z) = \rho_d - (\rho_d - \rho_s)e^{-z/H} \tag{1}$$

where $\rho_s = 1100$ kg m^{-3} and $\rho_d = 1800$ kg m^{-3}. Fig. 1 shows the H-parameters of the lunar regolith media [5].

B. Physical Temperature Derived From the Heat Conduction

The heat conduction equation is to be solved to describe the physical temperature with media thermal properties [8]

$$\rho C\frac{\partial T}{\partial t} = \frac{\partial}{\partial z}\left(K\frac{\partial T}{\partial z}\right) \tag{2}$$

where $\rho(z)$ is the bulk density, C is the heat capacity of the media, $T(z)$ is the temperature, and K is the thermal conductivity of the regolith media. Based on the measurement of returned samples, the heat capacity was found to be temperature dependent and an empirical polynomial was derived as [9], [10]

$$C = C_0 + C_1T + C_2T^2 + C_3T^3 + C_4T^4 \tag{3}$$

where $C_0 = -3.6125\text{Jkg}^{-1}\text{K}^{-1}$, $C_1 = +2.7431\text{Jkg}^{-1}\text{K}^{-2}$, $C_2 = +2.3616 \times 10^{-3}\text{J kg}^{-1}\text{K}^{-3}$, $C_3 = -1.2340 \times 10^{-5}\text{J kg}^{-1}\text{K}^{-4}$, and $C_4 = +8.9093 \times 10^{-9}\text{J kg}^{-1}\text{K}^{-5}$. It was understood that C is not sensitive to different samples [11].

It has been studied that the thermal conductivity consists of solid phonon conductivity and radiative conductivity with a dimensionless parameter χ as follows:

$$K = K_c\left[1 + \chi\left(\frac{T}{350}\right)^3\right] \tag{4}$$

where $\chi = 2.7$. K_c is the solid phonon thermal conductivity. Based on the experimental data in [12], K_c is assumed to be linearly proportional to the density

$$K_c = K_d - (K_d - K_s)\frac{\rho_d - \rho}{\rho_d - \rho_s} \tag{5}$$

where $K_s = 7.4 \times 10^{-4}\text{W m}^{-1}\text{K}^{-1}$ and $K_d = 3.4 \times 10^{-3}\text{W m}^{-1}\text{K}^{-1}$ are the heat conductivity at the surface and depth, respectively. With this thermal conductivity, the surface temperature at night can be fit.

The boundary conditions of (2) are written as

$$K(z,T)\frac{\partial T}{\partial z}\bigg|_{z=0} = \text{TSI}(1-A)\cos^+\theta_i - e\sigma T_s^4 - J_0 \tag{6a}$$

$$K(z,T)\frac{\partial T}{\partial z}\bigg|_{z=-\infty} = -J_0 \tag{6b}$$

where total solar irradiance (TSI) is the solar irradiance, and is determined by the distance between the sun and the moon. For example, as this distance is 1 AU (astronomical unit), TSI is about 1371 W/m^2 [13], and during aphelion and perihelion, TSI is taken as 1326 W/m^2 and 1418 W/m^2, respectively. During day time, the surface is directly illuminated by intense solar irradiance, and such heat energy directly from the sun is much larger than the heat conducted to the deep layer. In this paper, TSI is set to the average value, 1371 W/m^2. The parameter e of (6a) is the bolometric IR emissivity of lunar surface, and is set to 0.95 [14]. T_s is the surface temperature and J_0 is the heat flow and is set to 0.018 W/m^2 [15]. θ_i is the incident angle of sunlight. When θ_i is less than 90° during day time, $\cos^+\theta_i$ is equal to $\cos\theta_i$, otherwise, $\cos^+\theta_i$ is zero. In this paper, the topography of lunar surface is described by the DEM and θ_i is the local incident angle [8].

The lunar surface albedo A has the dependence upon solar incident angle and is empirically formulated as follows [16]:

$$A(\theta) = A_0 + a(\theta/45)^3 + b(\theta/90)^8 \tag{7}$$

where A_0 is the normalized albedo, derived by dividing Clementine 750 nm data with a factor of 1.3 to an average solar wavelength. The albedo is in good agreement with the result derived from Diviner's broadband solar channels [4]. The parameters a and b are two empirical coefficients, estimated as 0.06 and 0.25 [5]. Average A_0 along the equator is 0.134.

Fig. 2 shows the solar albedo of a center region of the lunar surface, where the Diviner data at T_7 channel over the areas of (0°N–2°N, 2°W–0°E) are chosen for validation of aforementioned thermo-physical parameters. The average A_0 of this area is 0.09 from Clementine 750 nm data and the

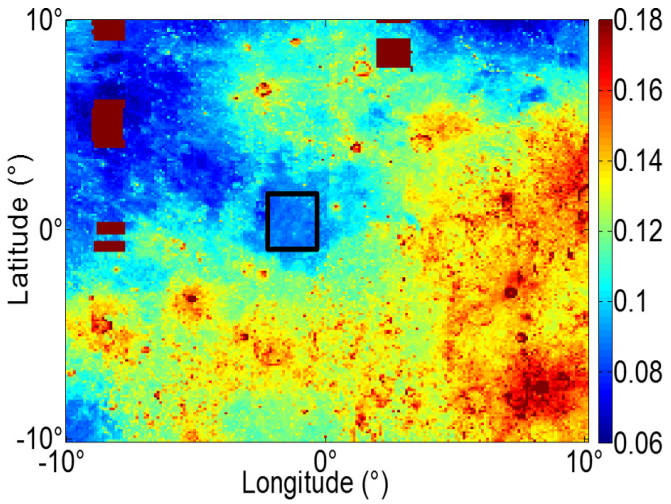

Fig. 2. Solar albedo of lunar center region. Diviner data inside the black box are chosen to validate the heat transfer equation.

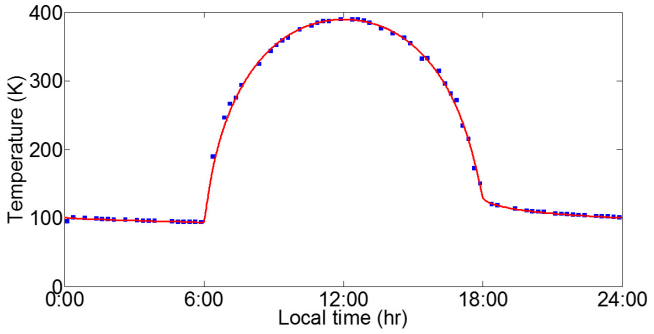

Fig. 3. Validation of the heat conduction model. The solid red line is the simulated surface temperature and the blue points are the average temperatures of Diviner T_7 channel.

average H is 0.06 m from Fig. 1. The average slope angle of this area is set to be 0° as a flat surface from DEM.

Based on aforementioned parameters, e.g., a, b of (7), H, K of (1) and (2), numerical finite-difference time-domain (FDTD) method is applied to solve (2) and (6) and obtain the temperature profile $T(z)$. In the MATLAB code of FDTD calculation, the time step δt and space step δz are chosen as 18 s and 0.001 m, respectively, which will meet the Fourier-von Neumann stability condition [5], [8], [25]

$$\frac{K\delta t}{\rho C \delta z^2} \leq \frac{1}{2}. \tag{8}$$

An initial temperature of 256 K was given for each cell. The Newton method is used to solve (6a) to acquire the surface temperature. FDTD code is then running for 300 lunations (29.53 earth day) to guarantee the convergence of the solution, which makes the temperature difference at the same local time between two successive lunar days is less than 0.0001 K.

Fig. 3 presents the lunar surface temperature versus lunar local time, where discrete points are from the Diviner data, as validation. Furthermore, the temperatures at different depths also match the data of Apollo heat-flow experiments [17], [18].

For example, at Apollo 15 probe 1 site, the temperature at the depth 1.38 m is 253 K, with the heat flow of 3×10^{-6} W/cm^2 [19]. Given that the solar albedo is 0.07,

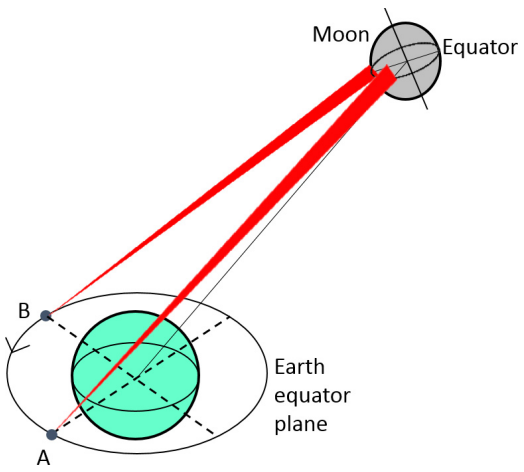

Fig. 4. FY-4M views the moon for thermal calibration.

which corresponds to the surface temperature of 379 K at noon, the simulated temperature at the depth 1.38 m is 251 K. At Apollo 17 probe site 2, the temperature at the depth 1.30 m is 256.11 K, with the heat flow 2.9×10^{-6} W/cm^2. Given the solar albedo 0.07, which corresponds to the surface temperature 384 K at noon, the simulated temperature at the depth 1.3 m is 255 K [19]. All these simulation results are well within the error band, 20%, of the Apollo experiments.

By the way, there are some rock stones distributed over the surface with higher temperature about tens of Kelvin at night. However, the percentage of those rock stones is much less than 1% [20], and is actually ignored (<1 K) [4]. In Fig. 3, the level 4 global cumulative products at the T_7 channel from Diviner data are employed.

Since the surface temperature and its profile in regolith media have been validated by Diviner data and Apollo temperature measurements, these temperatures and those derived thermo-physical parameters would be applied to calculation of microwave TB in Session IV and millimeter wave TB in Session V.

III. Millimeter-Wave FY-4M: Calibration by the Moon

FY-4M, as one of the series of geosynchronous meteorological satellites, is planning to upload multi-channel millimeter-wave radiometers. As illustrated in Fig. 4, FY-4M is to be located on the orbit altitude 35 800 km at the longitude around E99.5° ∼ E123.5° above the earth equator.

Calibration is usually conducted first in the T/V chamber before launch and then is repeated during operations on orbits [21]. There are hot-target and cold-target onboard the satellite, providing relative irradiances for calibration. However, due to the harsh conditions in the space, many uncertainties and instabilities will affect the calibration. TB of the lunar surface can keep very long-period stability due to no atmospheric interference and few random surface variations. It is a good candidate for thermal calibration during FY-4M operation. The distance between the moon and the earth varies between 363 400 km (perigee) and 405 400 km (apogee) [22]. It can be derived that such large distance makes the nadir

observation from FY-4M radiometer toward a center region of the lunar equator.

The observation beam from FY-4M expands from 0.097° to 0.027°. It is calculated that the coverages for different channels with observation diameters of 750 (55 GHz), 480 (89 and 118 GHz), 300 (166 and 183 GHz), and 210 km (425 GHz) at apogee. Thermal emission from these regions at noon time would be received by those multichannel radiometers of FY-4M.

IV. Loss Tangent Fitting and Microwave TB

The moon is modeled as the surface media of fine-grained regolith soil covering the bedrock [23], The thickness of the regolith layer is much larger than the penetration depth, e.g., of 37 GHz or higher frequencies [24], [6]. So, in thermal emission modeling for high-frequency channels, lunar layer can be simplified as a semiinfinite regolith media [25]. Based on the fluctuation–dissipation theorem and WKB approach, TB from a uniform inhomogeneous medium can be obtained [26], [27]. At nadir observation, it can be simplified as

$$T_B(0) = [1 - R(0)] \int_0^\infty \kappa_a(z) T(z) e^{-\int_0^z \kappa_a(z')dz'} dz \tag{9}$$

where $R(0)$ and $[1 - R(0)]$ are the reflectivity and the emissivity at nadir observation. There is

$$R(0) = \left(\frac{1 - \sqrt{\varepsilon_s}}{1 + \sqrt{\varepsilon_s}} \right)^2 \tag{10}$$

where ε_s is the surface dielectric constant of the regolith and can be obtained by (16) with $\rho(0)$ of (15). It is found that slopes may make the local observation over each meshed region in the scale of spatial resolution away from nadir direction, but it is very trivial and negligible. The absorption coefficient of the regolith media, κ_a, is derived as

$$\kappa_a = \frac{2\pi f \varepsilon''(z)}{c\sqrt{\varepsilon'(z)}} \tag{11}$$

where f is the frequency, c is the light speed in free space, and $\varepsilon'(z)$ and $\varepsilon''(z)$ are the real and imaginary parts of the dielectric constant of the regolith at the depth z, respectively. The ratio $\varepsilon''(z)/\varepsilon'(z) = \tan\delta$ is defined as the loss tangent, which is a key parameter to (11) and TB simulation.

A. Dielectric Constant of Regolith Media

The real $\varepsilon'(z)$ is derived from the density profile of soil, $\rho(z)$, which is related with porosity profile $n(z)$ and the abundance of FeO,TiO_2. The loss tangent $\tan\delta$ was empirically formulated with fitting data of TiO_2[28], [29].

Based on the Apollo measurements, the density profile at Apollo landing sites (specifically indicated by the subscript 0) was proposed as

$$\rho_0(z) = 1.919 \frac{z + 0.122}{z + 0.18}. \tag{12}$$

And the porosity profile of regolith media was written as

$$n(z) = 1 - \rho_0(z)/G_0 \tag{13}$$

where $G_0 = 3.1$ g/cm^3 is the nominal specific gravity (bulk density without void), based on the Apollo regolith samples. The porosity $n(z)$ is the average value and is then assumed to keep the same value at different places in this research as its influence on TB is minor and not much knowledge is available.

Generally, the specific gravity is related to mineral abundance at that location [30]

$$G = 27.3\text{FeO} + 11\text{TiO}_2 + 2773 \tag{14}$$

where G is in kg/m^3 and FeO and TiO_2 are the percentage of mineral by weight. The density profile $\rho(z)$ can be generally written as

$$\rho(z) = (1 - n)G. \tag{15}$$

As a composite media, following the Maxwell–Garnett formula [29], the real $\varepsilon'(z)$ is obtained by

$$\frac{1}{<\rho>} \frac{<\varepsilon> - 1}{<\varepsilon> + 2} = \frac{1}{\rho(z)} \frac{\varepsilon'(z) - 1}{\varepsilon'(z) + 2} \tag{16}$$

where the normalized $<\varepsilon> = 2.75$ with $<\rho> = 1.7$ g/cm^3 The dielectric constant $\varepsilon'(z)$ of regolith media is determined by (16) and $\rho(z)$ of (15).

B. Loss Tangent Fitting

However, a restricted test at 450 MHz in the earth lab was adopted to determine the loss tangent $\tan\delta$ based on only 23 samples with limited abundance of $TiO_2 > 4$ wt.% [29], as formulated as

$$\tan\delta = 10^{-2.395 + 0.064\text{TiO}_2}. \tag{17}$$

It is noted that abundance of TiO_2 in lunar regolith is usually >4 wt.%, e.g., in maria. The data test at 450 MHz and (17) are given by the red cross points and red lines in Fig. 5(a) and (b).

We specifically collect normalized CE-2 TB_{37} data along the lunar equator at noon time, the root-mean-squares (RMSs) of which are within 0.5 K in the prelaunch calibration [31], to invert $\tan\delta$ versus TiO_2[32], and formulate the relationship as follows:

$$\tan\delta = 3.516 \times 10^{-4}\text{TiO}_2 + 0.0087 \text{ as } \text{TiO}_2 > 1\% \tag{18a}$$

$$\tan\delta = -8.945 \times 10^{-5}\text{TiO}_2 + 0.0097 \text{ as } \text{TiO}_2 < 1\% \tag{18b}$$

where TiO_2 is in wt.%.

Linear fitting of (18a) and (18b) are given by black points and black line in Fig. 5(a) and (b). The RMSEs between the inversed values and the fit values are both 0.001 for (18a) and (18b). CE-2 TB_{37} data on the lunar equator at noon and our corresponding simulation are presented in Fig. 6. It is counted that the points over 70% have the error less than 3 K, 88% less than 5 K, and almost all points (99.5%) less than 10 K.

In these simulations, the mineral abundance and solar albedo derived from Clementine data is 10 pixles/degree and there are 3600 pixels along the equator, and the resolution of DEM is 4 pixels/degree. A mean value of mineral abundance and solar albedo from Clementine data is taken by the step of 5 pixels so that there are 720 pixels along the equator. The temperature

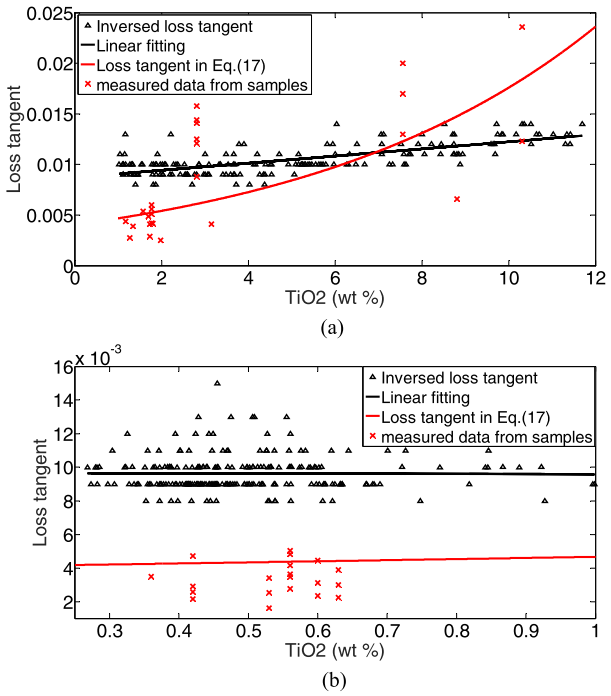

Fig. 5. Linear fitting of loss tangent. (a) $TiO_2 > 1$. (b) $TiO_2 < 1$. The black triangles are the inversed loss tangents. The black line is the result of linear fitting. The red line is the loss tangent of (17).

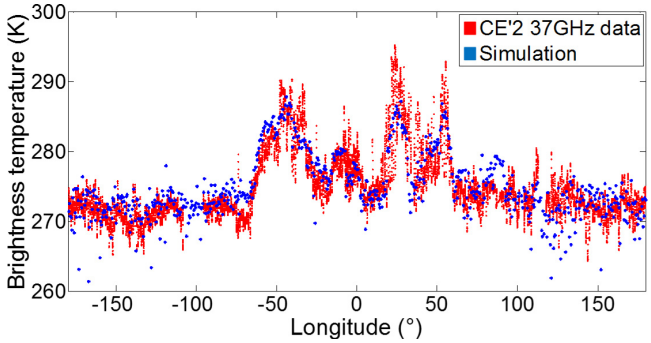

Fig. 6. Comparison between CE-2 37GHz MRM data and simulated TBs. The red points are CE-2 data and the blue points are the simulated data. CE-2data are available online: http://moon.bao.ac.cn/searchOrder_pds.search.

profiles at every point is obtained with solar albedo and slopes derived from DEM.

The real $\varepsilon'(z)$ is obtained from (14)–(16). The mean values of CE-2 TB_{37} data are derived within the corresponding longitude span to invert $\tan\delta$, as shown in Fig. 5(a) and (b). The exhaustion method of $\tan\delta$ within the range from 0.004 to 0.017 with a gap of 0.001 is used to ensure a satisfied $\tan\delta$ at each point. The 59% of total points along the equator have small TiO_2 abundance, less than 1%. In order to make good fitting, $\tan\delta$ of $TiO_2 < 1$ and $TiO_2 > 1$ are fit, respectively. The least-squares method is used for linear fitting. Based on (18a) and (18b) and our TB simulation, the approach is also extended to other latitudes, for example, 60°N, for further validation. Comparison of CE-2 TB_{37} data and our simulation are presented in Fig. 7. To count the errors in comparison of Fig. 7, for example, it is found that there is 87% of the points

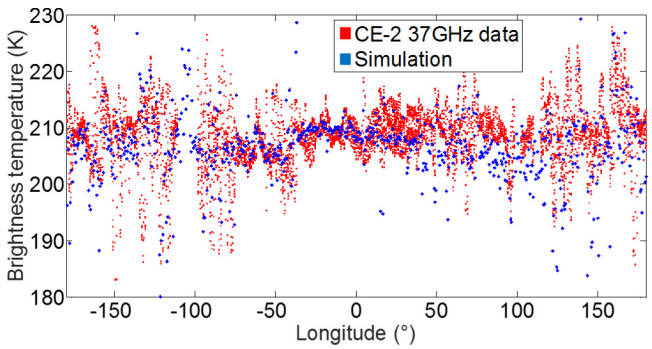

Fig. 7. Comparison between CE-2 TB_{37} and simulated TB at latitude 60°N. The red points are CE-2 data and the blue points are the simulated data.

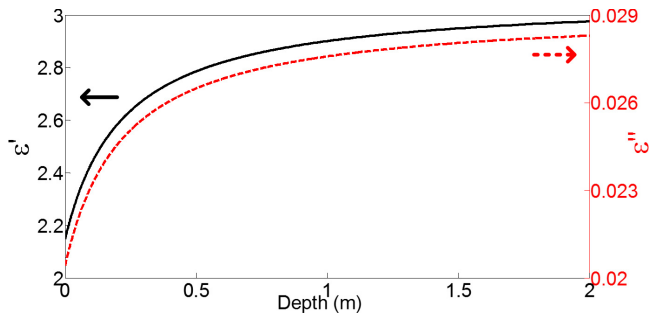

Fig. 8. Complex dielectric constant of the regolith as a function of depth.

with error less than 10 K, 63% of the points with error less than 5 K, and 44% of the points with error less than 3 K.

The penetration depth d of radar wave is given as [33]

$$d = \frac{c\sqrt{\varepsilon'}}{2\pi f \varepsilon''}. \tag{19}$$

It can be seen that the large $\tan\delta$ leads to a small penetration d and makes higher TB at noon in maria, and as usually with large $\tan\delta$ than highland. Furthermore, the solar albedo in maria about 0.08 is lower than that of highland, and may raise the temperature about 8 K. In Fig. 6, for example, TB_{37} at the longitude $-50°$ of a maria can be raised about 15 K, where 8 K is caused due to lower solar albedo and the rest 7 K is due to high $\tan\delta$. Based on the average abundance FeO = 8.9%,TiO_2 = 2.3%, along the equator, Fig. 8 shows the complex dielectric constant $\varepsilon'(z)$ and $\varepsilon''(z)$.

V. Brightness Temperature of Lunar Regions

Now, we extend our TB simulation with all aforementioned parameters to millimeter waves of FY-4M. Fig. 9(a) and (b) shows the TB along the equator at noon and midnight, respectively. Longitude indicates the center of the region of the lunar equator. The region size for each channel is given in Section III.

The error bars indicate possible variance if other varying parameters in this region were chosen for calculations of the temperature and dielectric property. The error of 55 GHz may be the largest because of its largest observed region.

In comparison of Fig. 9(a) and (b), it can be seen that the sequence from high to low TB is converse at noon and night,

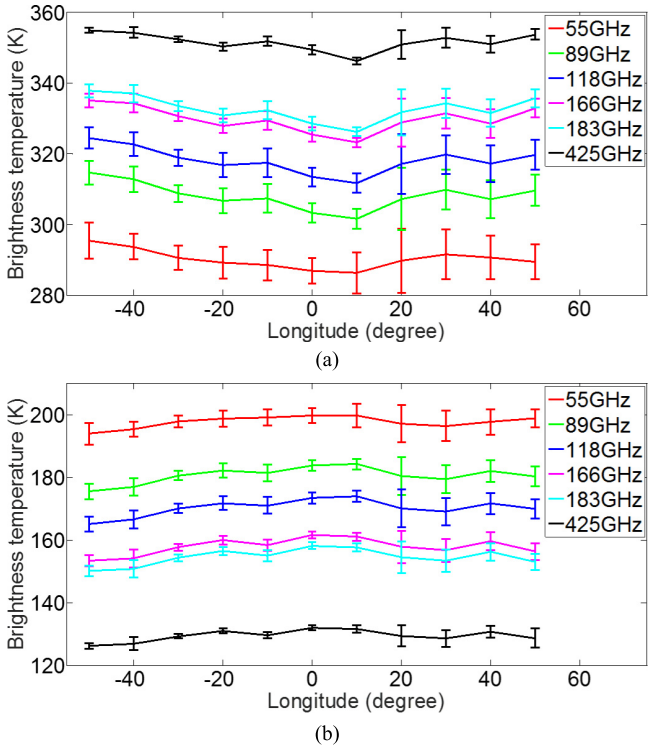

Fig. 9. Average TB of lunar equator at (a) noon and (b) midnight. The error bars are standard error of the TB in the observation area.

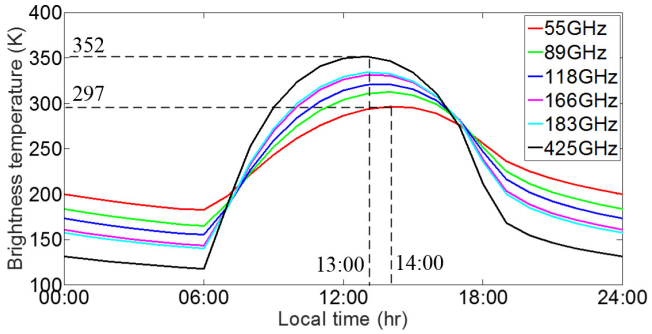

Fig. 10. TB of 24 local hours on a center region of lunar equator.

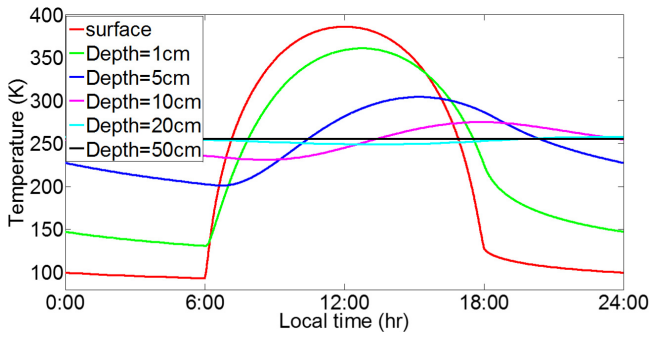

Fig. 11. Temporal variation of temperature of regolith at different depth when heat is conducting into the media.

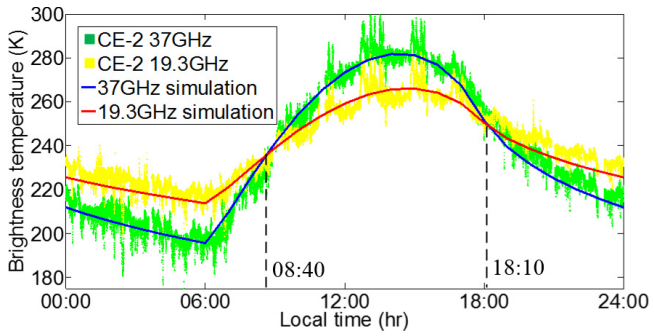

Fig. 12. Intersections of TBs at different frequency. Green and yellow points are the CE-2 MRM 37 and 19.3 GHz data along the equator. Solid lines are the simulation results.

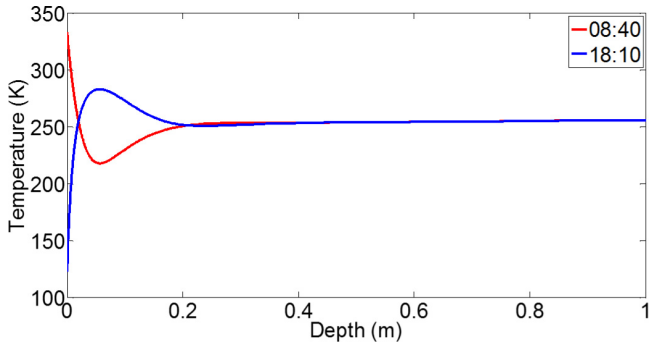

Fig. 13. Temperature profiles at crossing time 08:40 and 18:10.

because of solar irradiance in day time and TB sensitivity of different channel to different penetration depth. It is similar to Fig. 6 of 37 GHz, Fig. 9(a) shows TB of maria higher than highland, and the highest TB is around 50°W (Oceanus Procellarum) and 30°E (Mare Tranquillitatis), while the lowest TB appears near 10°E. However, TB at night is reversed, i.e., TB of maria is lower than highland, and meanwhile large penetration depth of low frequency makes TB higher at night.

Fig. 10 shows TB variation during 24 local hours of the center region of lunar equator. It can be seen that when day time comes, solar irradiance significantly raises the lunar surface temperature, and then as night comes, the temperature quickly cools down. When TB steadily reaches the steady peak, it might be a good time to make TB calibration. As no sun illumination and night comes, quick cooling down may not good for quantitative calibration.

It is interesting to find that the time when TB reaches peak is different for different channels, not exactly at 12:00. Lower frequency with deeper penetration depth would more shift the peak time a litter later when the heat is conducted to deeper media. Fig. 11 describes temporal variation of physical temperature at different depths of lunar regolith, when the heat is conducted into the media.

In Fig. 10, it might be interesting to find the cross points of multichannel TB around 07:30 AM and 17:30 PM of lunar day. At this cross time, TB of all these channels is almost similar. It might be a way to check and evaluate the performance each channel for calibration/validation. This phenomenon is due to the heat conduction and peak shift, as explained in Figs. 10 and 11.

This phenomenon also appears in CE-2 data, e.g., TB_{37} and TB_{19} along lunar equator, as shown in Fig. 12. Both CE-2 TB data and simulation are presented. Its temperature profiles at the crossing time are given in Fig. 13.

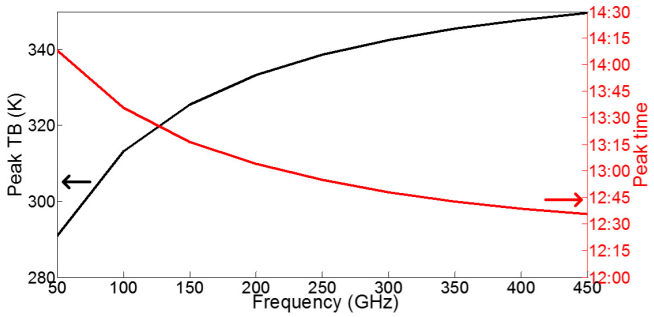

Fig. 14. Peak values and peak time of TB for all FY-4M channels.

In Fig. 13, it can be seen that as sunlight begins illuminate the lunar surface, surface temperature raises quickly in morning. Then, heat is gradually conducted to underneath cool regolith media. As night is coming, the surface temperature quickly cools down (see blue line) after 18:00, but the temperature of underneath media more or less keeps warm. A turning point is around the depth 0.1 m.

VI. Discussion

A. Influence of Thermo-Physical and Dielectric Properties

To model the lunar regolith media, the thermo-physical and dielectric parameters are the key issues. The influence of thermo-physical parameters, like heat conductivity and H-parameter, on simulated TBs are analyzed. For example, let K_s and K_d vary in the range of $(6.4 \times 10^{-4}\mathrm{Wm}^{-1}\mathrm{K}^{-1}$–$8.4 \times 10^{-4}\mathrm{Wm}^{-1}\mathrm{K}^{-1})$ and $(2.4 \times 10^{-3}\mathrm{Wm}^{-1}\mathrm{K}^{-1}, 4.4 \times 10^{-3}\mathrm{Wm}^{-1}\mathrm{K}^{-1})$, respectively, based on our calculations of TB on the lunar equator, it affects the surface temperature at night less than 3 K, and affects all TB of FY-4M channels less than 2.5 K. The H-parameter along the lunar equator is in the range of 0.055–0.065 m, which may affect the surface temperature and TB less than 1 K. In this paper, the simulation of physical temperature with these parameters has been validated by Diviner data and Apollo heat flow measurement.

To take into account of dielectric property $\varepsilon(z)$, the typical mineral abundance of maria, $\mathrm{TiO}_2 = 6\%$, $\mathrm{FeO} = 15\%$ and of highland, $\mathrm{TiO}_2 = 0.5\%$, $\mathrm{FeO} = 4\%$ are taken as an example. It is found that the real part ε' affects all TB less than 2.5 K, but the imaginary part ε'', or loss tangent $\tan\delta$, are especially important. For example, if $\tan\delta = 0.009$, the TB are 342.88 (425 GHz), 321.90 (183 GHz), 318.80 (166 GHz), 307.1 (118 GHz), 297.00 (89 GHz), and 280.53 K(55 GHz); and if $\tan\delta = 0.013$ the TB are 348.64 (425 GHz), 332.43 (183 GHz), 329.84 (166 GHz), 319.65 (118 GHz), 310.13 (89 GHz), and 292.95 K (55 GHz). Difference is in the range of 6–12 K. We employ CE-2 TB_{37} data to formulate (18) and make fitting $\tan\delta$ with the RMSE 0.001. The uncertainty is less than 1.8 (425 GHz), 3.2 (183 GHz), 3.4 (166 GHz), 3.7 (118 GHz), 3.8 (89 GHz), and 3.4 K(55 GHz).

B. Advise for Calibration

As shown in Fig. 10, the time when TB reaches the peak is different for different channel because of different penetration depth. Fig. 14 gives the peak value and peak time for each channel. TB of higher frequencies has larger peak values and reaches the peak earlier. TB peaks of each channel are suitable for calibration, and meanwhile, TB at night is alternative cold targets as well for calibration. In addition, it is interesting to find in Fig. 10 that the TB of different frequencies is crossed at a certain local times, e.g., local time 07:00 and 18:00. It might be useful to evaluate and compare TB and performance of all FY-4M channels.

VII. Conclusion

TB of lunar surface is under study for calibration of multichannel millimeter-wave radiometers, which are planning to be uploaded on geosynchronous satellite FY-4M. Since TBs of lunar surface keep long period stability and all thermo-physical and dielectric properties at certain time and location can be accurately determined. Based on uniformly inhomogeneous model with bulk density profile and conduction parameters to solve the heat transfer equation, physical temperature profile of regolith media is obtained and validated by the Diviner data. The loss tangent can be fit and validated by CE-2 37 GHz TB. Then, using fluctuation dissipation theorem, TB of regolith media at all FY-4M channels over the lunar equator regions are numerical simulated. These TB results are further analyzed for possible errors caused by the fit loss tangent. It can be seen that these TB on lunar equator surface at certain time and location, where all parameters can be determined, can be applied for calibration of FY-4M multi-channels radiometers.

When TB reaches the peak and slowly varies, it is recommended for calibration. In contrast, TB around 06:00 is rapidly increased and is not good for calibration. Based on the parameterized model of lunar regolith, the loss tangent of the lunar media may cause the TB error, in the range of 1.8 (425 GHz) to 3.8 K (89 GHz). The error is sustainable. It is also interesting to find the crossing time of all TB of FY-4M due to the peak shift caused by different penetration depths for different channels. It might be useful to evaluate the performance of all radiometer channels in calibration. It should be noted that as the radiometer frequency is very high, i.e., millimeter waves 425 GHz. Some uncertainties to determine the loss tangents based on our 37 GHz test might be remained for more discussion.

Acknowledgment

The authors would like to thank Dr. Q. Guo and N. Lu of the National Satellite Meteorological Center, Beijing, China, for introduction of the FY-4M Project. They would also like to thank Dr. P. O. Hayne from the Jet Propulsion Laboratory, Pasadena, CA, USA, for inversed H-parameters.

References

[1] H. H. Kiefer, "Photometric stability of the lunar surface," *Icarus*, vol. 130, no. 2, pp. 323–327, 1997.
[2] J. H. Piddington and H. C. Minnett, "Microwave thermal radiation from the Moon," *Austral. J. Chem.*, vol. 2, no. 1, pp. 63–77, 1949.
[3] D. A. Paige *et al.*, "The lunar reconnaissance orbiter diviner lunar radiometer experiment," *Space Sci. Rev.*, vol. 150, pp. 125–160, Jan. 2010.
[4] A. R. Vasavada *et al.*, "Lunar equatorial surface temperatures and regolith properties from the diviner lunar radiometer experiment," *J. Geophys. Res., Planets*, vol. 117, no. E12, p. E00H18, 2012.
[5] P. O. Hayne *et al.*, "Global regolith thermophysical properties of the Moon from the Diviner Lunar Radiometer Experiment," *J. Geophys. Res., Planets*, vol. 122, no. 12, pp. 2371–2400, 2017.

[6] W. Fa and Y.-Q. Jin, "A primary analysis of microwave brightness temperature of lunar surface from Chang-E 1 multi-channel radiometer observation and inversion of regolith layer thickness," *Icarus*, vol. 207, no. 2, pp. 605–615, 2010.
[7] Y.-Q. Jin and W. Fa, "The modeling analysis of microwave emission from stratified media of nonuniform lunar cratered terrain surface for Chinese Chang-E 1 observation," *IEEE Geosci. Remote Sens. Lett.*, vol. 7, no. 3, pp. 530–534, Jul. 2010.
[8] S. Yu and W. Fa, "Thermal conductivity of surficial lunar regolith estimated from Lunar Reconnaissance Orbiter Diviner Radiometer data," *Planet. Space Sci.*, vol. 124, pp. 48–61, May 2016.
[9] M. J. Ledlow, J. O. Burns, G. R. Gisler, J.-H. Zhao, M. Zeilik, and D. N. Baker, "Subsurface emissions from Mercury-VLA radio observations at 2 and 6 centimeters," *Astrophys. J.*, vol. 384, pp. 640–655, Jan. 1992.
[10] B. S. Hemingway, K. M. Krupka, and R. A. Robie, "Heat capacities of the alkali feldspars between 350 and 1000 K from differential scanning calorimetry, the thermodynamic functions of the alkali feldspars from 298. 15 to 1400 K, and the reaction quartz + jadeite = analbite," *Amer. Mineralogist*, vol. 66, nos. 11–12, pp. 1202–1215, 1981.
[11] B. S. Hemingway, R. A. Robie, and W. H. Wilson, "Specific heats of lunar soils, basalt, and breccias from the Apollo 14, 15, and 16 landing sites, between 90 and 350 °K," in *Proc. Lunar. Sci. Conf.*, vol. 4, 1973, p. 2481.
[12] J. A. Fountain and E. A. West, "Thermal conductivity of particulate basalt as a function of density in simulated lunar and Martian environments," *J. Geophys. Res., Planets*, vol. 75, no. 20, pp. 4063–4069, 1970.
[13] G. D. Racca, "Moon surface thermal characteristics for moon orbiting spacecraft thermal analysis," *Planet. Space Sci.*, vol. 43, no. 6, pp. 835–842, 1995.
[14] J. L. Bandfield, P. O. Hayne, J.-P. Williams, B. T. Greenhagen, and D. A. Paige, "Lunar surface roughness derived from LRO Diviner Radiometer observations," *Icarus*, vol. 248, pp. 357–372, Mar. 2015.
[15] M. G. Langseth, S. J. Keihm, and K. Peters, "Revised lunar heat-flow values," in *Proc. Lunar Planet. Sci. Conf.*, 1976, pp. 3143–3171.
[16] S. J. Keihm, "Interpretation of the lunar microwave brightness temperature spectrum: Feasibility of orbital heat flow mapping," *Icarus*, vol. 60, no. 3, pp. 568–589, 1984.
[17] S. J. Keihm, K. Peters, M. G. Langseth, and J. I. Chute, "Apollo 15 measurement of lunar surface brightness temperatures thermal conductivity of the upper 1 1/2 meters of regolith," *Earth Planet. Sci. Lett.*, vol. 19, no. 3, pp. 337–351, 1973.
[18] S. J. Keihm and M. G. Langseth, Jr., "Surface brightness temperatures at the Apollo 17 heatflow site: Thermal conductivity of the upper 15 cm of regolith," in *Proc. Lunar Planet. Sci. Conf.*, vol. 4, 1973, p. 2503.
[19] M. G. Langseth, J. L. Chute, and S. Keihm, "Direct measurements of heat flow from the moon," in *Proc. Lunar Planet. Sci. Conf.*, vol. 4, 1973, p. 455.
[20] J. L. Bandfield, R. R. Ghent, A. R. Vasavada, D. A. Paige, S. J. Lawrence, and M. S. Robinson, "Lunar surface rock abundance and regolith fines temperatures derived from LRO Diviner Radiometer data," *J. Geophys. Res., Planets*, vol. 116, p. E00H02, Dec. 2011.
[21] Z. Wang, J. Li, S. Zhang, and Y. Li, "Prelaunch calibration of microwave humidity sounder on China's FY-3A Meteorological Satellite," *IEEE Geosci. Remote Sens. Lett.*, vol. 8, no. 1, pp. 29–33, Jan. 2011.
[22] J. Meeus, *Astronomical Algorithms*. Richmond, VA, USA: Willmann-Bell, 1991, pp. 325–332.
[23] G. Heiken, B. M. French, G. Heiken, and D. Vaniman, *Lunar Sourcebook: A User's Guide to the Moon*. New York, NY, USA: Cambridge Univ. Press, 1991, pp. 285–356.
[24] Y. G. Shkuratov and N. V. Bondarenko, "Regolith layer thickness mapping of the Moon by radar and optical data," *Icarus*, vol. 149, no. 2, pp. 329–338, 2001.
[25] T. Fang and W. Fa, "High frequency thermal emission from the lunar surface and near surface temperature of the Moon from Chang'E-2 microwave radiometer," *Icarus*, vol. 232, pp. 34–53, Apr. 2014.
[26] Y.-Q. Jin, *Electromagnetic Scattering Modelling for Quantitative Remote Sensing*. Singapore: World Scientific, 1993, p. 310.
[27] F. T. Ulaby, R. K. Moore, and A. K. Fung, "Microwave remote sensing active & passive—Microwave remote sensing fundamentals and radiometry," NASA, Washington, DC, USA, Tech. Rep., 1981, pp. 229–230.
[28] P. G. Lucey, D. T. Blewett, and B. L. Jolliff, "Lunar iron and titanium abundance algorithms based on final processing of Clementine ultraviolet-visible images," *J. Geophys. Res., Planets*, vol. 105, no. E8, pp. 20297–20305, 2000.
[29] W. Fa and M. A. Wieczorek, "Regolith thickness over the lunar nearside: Results from Earth-based 70-cm Arecibo radar observations," *Icarus*, vol. 218, no. 2, pp. 771–787, 2012.
[30] Q. Huang and M. A. Wieczorek, "Density and porosity of the lunar crust from gravity and topography," *J. Geophys. Res., Planets*, vol. 117, no. E5, p. E05003, 2012.
[31] Z. Wang *et al.*, "Prelaunch calibration of Chang'E-2 lunar microwave radiometer," in *Proc. Int. Conf. Microw. Millim. Wave Technol.*, May 2010, pp. 1551–1554.
[32] Y.-C. Zheng, K. T. Tsang, K. L. Chan, Y. L. Zou, F. Zhang, and Z. Y. Ouyang, "First microwave map of the moon with Chang'E-1 data: The role of local time in global imaging," *Icarus*, vol. 219, no. 1, pp. 194–210, May 2012.
[33] W. Z. Fa, "Simulation for Ground Penetrating Radar (GPR) study of the subsurface structure of the Moon," *J. Appl. Geophys.*, vol. 99, pp. 98–108, Dec. 2013.

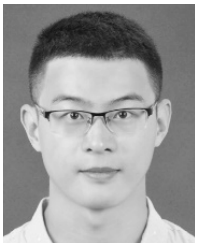

Niutao Liu was born in Jiangsu, China, in 1994. He received the B.S. degree from the Nangjing University of Posts and Telecommunications, Nanjing, China, in 2016. He is currently pursuing the Ph.D. degree with the School of Information Science and Engineering, Fudan University, Shanghai, China.

His research interests include planetary remote sensing, computational electromagnetics, and target recognition.

Wenzhe Fa (M'15) received the B.S. degree in applied physics from Xidian University, Xi'an, China, in 2003, and the Ph.D. degree in microwave remote sensing from Fudan University, Shanghai, China, in 2009.

From 2009 to 2011, he was a Post-Doctoral Fellow at the Institute de Physique du Globe de Paris, Paris, France. From 2011 to 2017, he was an Assistant Professor with the School of Earth and Space Sciences, Peking University, Beijing, China, where he is currently the tenured Associate Professor. He has authored over 30 papers in peer-reviewed journals. His research interests include microwave remote sensing, lunar and planetary sciences, and impact cratering.

Dr. Fa is a member of the Lunar Volatile Specific Action Team, the Lunar Exploration Analysis Group. He was a recipient of the Second Class National Nature Science Ais now the ward of China in 2011. He currently serves as an Associate Editor of the *Journal of Geophysical Research–Planets*.

Ya-Qiu Jin (SM'89–F'04–LF'18) received the degree in atmospheric physics from Peking, Beijing, China, in 1970, and the M.S., E.E., and Ph.D. degrees in electrical engineering and computer science from the Massachusetts Institute of Technology, Cambridge, MA, USA, in 1982, 1983, and 1985, respectively.

In 1985, he joined Atmospheric Environmental Research, Inc., Cambridge, MA, USA, as a Research Scientist, a Research Associate Fellow at the City University of New York, New York, NY, USA, from 1986 to 1987 and a Visiting Professor at the University of York, York, U.K., in 1993, sponsored by the U.K. Royal Society. He is currently the Te-Pin Professor and the Director of the Key laboratory for Information Science of Electromagnetic Waves, Institute of EM Big data and Intelligence Remote Sensing, Fudan University, Shanghai, China. He has authored over 760 papers in refereed journals and conference proceedings and 14 books, including the *Polarimetric Scattering and SAR Information Retrieval* (Wiley and IEEE, 2013), the *Theory and Approach of Information Retrievals from Electromagnetic Scattering and Remote Sensing* (Springer, 2005), and the *Electromagnetic Scattering Modeling for Quantitative Remote Sensing* (World Scientific, 1994). His research interests include electromagnetic scattering and radiative transfer in complex natural media, microwave satellite-borne remote sensing, as well as theoretical modeling, information retrieval and applications in earth terrain and planetary surfaces, and computational electromagnetics.

Dr. Jin is the fellow of TWAS (the Developing Countries Academy of Sciences), the International Academy of Astronautics, the Academician of the Chinese Academy of Sciences. He was an IEEE GRSS Distinguished Speaker and an Associate Editor of the IEEE ACCESS. He was a Co-Chair of TPC for IGARSS2011 in Vancouver, Canada, and the Co-General Chair for IGARSS2016 in Beijing, China. He was an Associate Editor of the IEEE TRANSACTIONS ON GEOSCIENCE AND REMOTE SENSING FROM 2005 to 2012 and the member of IEEE GRSS AdCom and Chair for IEEE Fellow Evaluation of GRSS from 2009 to 2011. He is now the Member of IEEE GRSS Major Awards Committee. He was a recipient of the Senior Research Associateship in NOAA/NESDIS by USA National Research Council, in 1996, the IEEE GRSS Distinguished Achievement Award in 2015, the IEEE GRSS Education Award in 2010, the China National Science Prize in 2011 and 1993, the Shanghai Sci/Tech Gong-Cheng Award in 2015, the first-grade MoE Science Prizes in 1992, 1996, and 2009 among many other prizes.